First-principles determination of magnetic properties of $CoCp_2$ on the Cr(001) surface

S. B. Song,[1] Z. Wang,[1] J. Li,[2] and R. Q. Wu[2,*]

[1]*State Key Laboratory of Surface Physics, Key Laboratory of Computational Physical Sciences, and Department of Physics, Fudan University, Shanghai 200433, China*

[2]*Department of Physics and Astronomy, University of California, Irvine, California 92697, USA*

(Received 12 September 2021; revised 9 January 2022; accepted 27 January 2022; published 10 February 2022)

Through density-functional calculations, we systematically studied the exchange bias effect of the antiferromagnetic Cr(001) substrate on a single magnetic molecule $CoCp_2$. The magnetic moment and magnetic anisotropy of $CoCp_2$ are largely tuned by the charge transfer between the molecule and substrate. A large exchange energy of ∼94 meV is found, which essentially pins the spin orientation of $CoCp_2$. This makes $CoCp_2$/Cr(001) an ideal combination for quantum sensing as its quantum spin states are well decoupled from those of the target magnetic entities. This work paves a way for the development of local quantum sensing with scanning probe techniques.

DOI: 10.1103/PhysRevB.105.064415

I. INTRODUCTION

Single-molecule magnets (SMMs) have attracted tremendous research interest since the macroscopic quantum tunneling of magnetization was demonstrated in a Mn_{12} acetate crystal [1,2]. The quantum effects in their well-confined structures [3,4] produce many intriguing phenomena that may have great potential for technological innovations, such as high-density data storage, spin filtering, and quantum information processing [5–7]. Many SMMs have been synthesized and characterized in recent years [8], and it was found that some of them have large magnetic anisotropy energies (MAEs) and hence high blocking temperatures [9,10]; some of them have long excited-spin state lifetimes and long coherence times of quantum spin states [11–13]. For the development of spin detection techniques, it is desired to use SMMs as sensors for achieving high spectroscopic and spatial sensitivities. For example, scanning probe microscopes may allow sensing quantum spin spectra of single atoms or molecules with a magnetic molecule nickelocene ($NiCp_2$, where Cp represents cyclopentadienyl) attaching on the apex of a scanning probe tip. A recent application of this technique successfully established a three-dimensional map of the exchange interaction between two nickelocene molecules in a continuously tunable fashion with a subangstrom resolution [14,15]. The spin polarization of magnetic atoms has also been explored by the scanning tunneling microscope (STM) with a tip that is functionalized by a $NiCp_2$ molecule [16]. However, two similar molecules with close MAEs have strong quantum coupling and the inelastic electron tunneling spectroscopy (IETS) is typically complex for interpretation [17]. In many cases, it is better to fix the magnetization of the probing molecule as a reference for the determination of spin polarization and spin excitation of targets. Obviously, one may use molecules with high MAEs or pin their magnetization with an antiferromagnetic (AFM) substrate or tip via the exchange bias effect [18]. Furthermore, an AFM substrate or tip does not produce much stray field on the target, especially with a SMM in the between. So far, magnetic properties of molecules on AFM substrates have rarely been studied. This inspires us to explore properties of magnetic molecules like $NiCp_2$ and $CoCp_2$ on an AFM substrate for the development of a new capability of local quantum sensing.

In this work, we systematically investigated the magnetic properties of $TMCp_2$/Cr(001) (TM = Co, Ni) using the first-principles calculations. Unlike on the Cu(100) and Ag(110) surfaces, the $NiCp_2$ molecule shows a structural instability on the Cr(001) surface and its spin-triplet state is strongly altered (see Fig. S1 and Table S1 in Supplemental Material) [19]. On the contrary, the $CoCp_2$ molecule is stable on Cr(001), and both its magnetic moment and MAEs are significantly affected through interacting with the substrate. Because of the exchange bias effect, the spin of $CoCp_2$ is essentially pinned by the substrate, which makes $CoCp_2$/Cr(001) suitable for probing spin states of different targets with a ultrahigh spatial resolution. Our work provides guidelines for the further development of the single-molecule spin sensor.

II. MODELS AND METHODS

As shown in Fig. 1, eight Cr layers and a vacuum 15 Å thick along the surface normal were used to mimic the Cr(001) surface. To give a single-molecule adsorption environment, we used a 4×4 supercell (11.52×11.52 Å^2) in the lateral plane and placed the $TMCp_2$ molecule on the top, hollow, and bridge sites on Cr(001). Since the Cr(001) surface has an in-plane ferromagnetic (FM) order and an interlayer AFM order [20], we also considered the FM and AFM coupling between the molecule and the topmost Cr atoms.

All density-functional theory (DFT) calculations were performed using the projector augmented-wave [21,22]

*wur@uci.edu

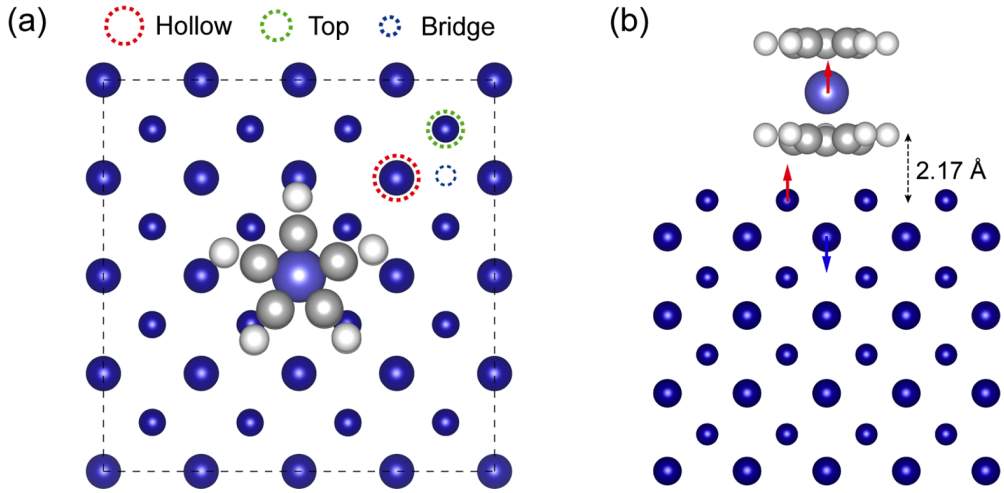

FIG. 1. (a) Top view and (b) side view of the $CoCp_2$/Cr(001) system. Blue spheres are the Cr atoms, white spheres the H atoms, gray spheres the C atoms, and purple spheres the Co atoms. Three adsorption sites are marked with different circles. The arrows represent atomic collinear magnetic moments.

formalism as implemented in the Vienna *Ab initio* Simulation Package [23,24]. The exchange-correlation potential was described within the framework of the spin-polarized generalized gradient approximation with the Perdew-Burke-Ernzerhof functional [25]. The van der Waals corrections in the form of DFT-D3 method [26] were incorporated in all calculations. The energy cutoff for the plane-wave basis expansion was set to 550 eV. The structural relaxations were performed using the conjugate gradient method with a criterion that requires the force on each unfixed atom smaller than 0.01 eV/Å. The $3 \times 3 \times 1$ and a $6 \times 6 \times 1$ Monkhorst-Pack meshes were used to sample the Brillouin zone for calculating the collinear and noncollinear magnetic configurations, respectively. The atomic magnetic moments were computed by Bader charge analysis scheme [27]. Different Hubbard U values were tested for the determination of magnetic states (see Fig. S2) [19] and the variation of U in a reasonable range was found to be insignificant in results. Besides, a structural model with seven Cr layers was also considered and results remain almost unchanged (see Tables S1 and S2) [19]. Without losing generality, we focus on results with $U = 0$ eV for a model with eight Cr layers in the following discussions.

III. RESULTS AND DISCUSSION

A. Geometrical and magnetic properties of $CoCp_2$/Cr(001)

As $NiCp_2$/Cr(001) is structurally unstable due to the strong interaction with Cr surface, we provide some of its properties in Supplemental Material [19] and mainly discuss $CoCp_2$/Cr(001). The stability of different adsorption geometries of cobaltocene is characterized by the adsorption energy defined as $E_{ad} = E[CoCp_2/Cr(001)] - E[CoCp_2] - E[Cr(001)]$. Here, $E[CoCp_2/Cr(001)]$, $E[CoCp_2]$, and $E[Cr(001)]$ represent the total energies of the $CoCp_2$/Cr(001), the isolated $CoCp_2$ molecule, and the bare Cr(001) surface, respectively. Furthermore, the magnetic coupling between the $CoCp_2$ molecule and the topmost Cr atoms is characterized by the exchange energy defined as $E_{ex} = (E_{FM} - E_{AFM})/2$, where E_{FM} and E_{AFM} represent the total energies of the FM and AFM configurations, respectively. From the results of fully relaxed structures listed in Table I, one may see that the $CoCp_2$ molecule prefers to take the hollow site on the Cr(001) surface with a sizable adsorption energy of -1.68 eV, indicating a strong molecule-substrate interaction. Meanwhile, the optimized distance between the lower pentagon of $CoCp_2$ and substrate is 2.17 Å.

The magnetic moments of Co atom and entire $CoCp_2$ molecule before and after adsorption are shown in the last two rows of Table I. The magnetic moments of the Co atom and the Cp rings in an isolated cobaltocene are 0.75 μ_B and 0.25 μ_B, respectively, giving a total magnetic moment of 1.0 μ_B ($S = 1/2$). On the Cr(001) surface, the magnetic moments of $CoCp_2$ and the Co atom increase to 1.89 μ_B and 1.31 μ_B, shifting toward the $S = 1$ state. Importantly, $CoCp_2$ molecule prefers to couple ferromagnetically with the surface Cr atoms. From the spin density in Fig. 2(a), one may see strong spin polarization in all parts of the molecule as well as over the surface Cr atoms. The planar averaged spin-density difference in Fig. 2(b) clearly indicates the enhancement of the magnetic moment of the Co atom.

As shown in Fig. 2(c), the charge-density difference reveals that significant orbital hybridization and electron redistribution occur at the interface. While the top Cp ring is not much affected, the π orbitals of the lower Cp ring take electrons

TABLE I. The adsorption energy (E_{ad}), the distance between the molecule and the substrate (d), the spin magnetic moments of the Co atom (M_{Co}) and the $CoCp_2$ molecule (M_{tot}) before and after adsorption.

	Free	Hollow	Top	Bridge
E_{ad} (eV)		−1.68	−1.62	−1.49
d (Å)		2.17	2.07	2.37
M_{Co} (μ_B)	0.75	1.31	0.77	0.97
M_{tot} (μ_B)	1.00	1.89	1.05	1.43

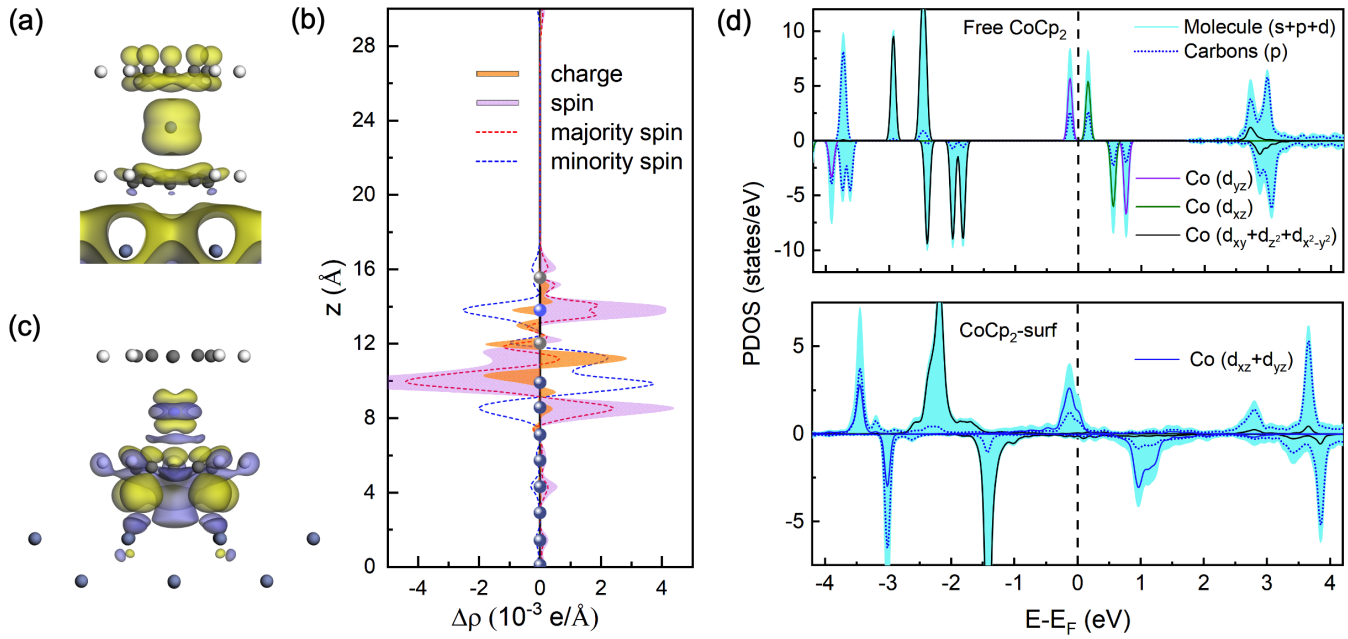

FIG. 2. Electronic structures of $CoCp_2$/Cr(001). (a) Spin-density isosurface (7.0×10^{-4}). (b) Planar average charge (orange), spin splits of charge (dashed lines), and spin- (purple) density differences along z direction: $\Delta\rho = \rho[CoCp_2/Cr(001)] - \rho[CoCp_2] - \rho[Cr(001)]$. The colored dots represent positions of atomic layers. (c) Charge-density difference isosurface (7.0×10^{-4}). Blue and yellow regions represent charge depletion and accumulation, respectively. (d) PDOS for the free $CoCp_2$ molecule and the $CoCp_2$ on a Cr(001) surface. The majority and minority spin channels are denoted by positive and negative PDOS, respectively. To show clearly, the degenerate Co-d orbitals were summed up. The vertical dashed line indicates the position of the Fermi level.

from the substrate. Meanwhile, electron rearrangement also occurs between Co-d orbitals, with the $t_{2g}(e_g)$ orbitals gaining (losing) electrons. The planar average of charge-density difference in the vertical direction in Fig. 2(b) also indicates the strong charge accumulation at the interface and the noticeable charge rearrangement within the molecule. By using the Bader charge analysis scheme [27], we found that 0.56 electrons are transferred from the four surface Cr atoms below the molecule to the C atoms at the interface, but the electron number of the Co atom is almost unchanged. The spin splits of $\Delta\rho$ indicate the charge swap from the minority spin channel to the majority spin channel at the Co and second Cr sites, and opposite swap at the topmost Cr site.

To further analyze the change of electronic structure, curves of the projected density of states (PDOS) are plotted in Fig. 2(d) for both the free and propped $CoCp_2$. Because the free $CoCp_2$ molecule has a D_{5h} symmetry, the eigenstates of the Co-d orbitals split into three groups: a singlet (d_{z^2}) and two doublets ($d_{xy,\ x^2-y^2}$ and $d_{yz,\ xz}$). However, the $d_{yz,\ xz}$ doublet is singly occupied in the majority spin channel, which is unfavorable according to the Jahn-Teller effect [28]. Therefore, a small distortion occurs to lift the orbital degeneracy and lower the total energy. As shown in the upper panel of Fig. 2(d), only the Co-d_{yz} orbital in the majority spin channel is occupied. The orbital splitting is less obvious in the case when the $CoCp_2$ molecule is placed on the Cr(001) surface due to the interaction and, as a result, the Co-d_{yz} and Co-d_{xz} orbitals in the majority channel are both partially occupied as shown in the lower panel of Fig. 2(d). Integrating over the DOS shows that the Co-d_{xz} orbital in the majority spin obtains about 0.25 e from the minority spin channel, as also suggested in the spin-split charge differences in Fig. 2(c). It is interesting that the enhanced magnetic moment is due to the local charge rearrangement between two spin channels, rather than due to the charge transfer from the substrate to the molecule. The surface Cr atoms donate their electrons mainly to the p orbitals of carbon atoms in the lower ring, and the PDOS curves of those carbon atoms show significant broadening near the Fermi level. As Co and carbon orbitals strongly hybridize in the entire energy range, the influence of the Cr substrate on the magnetization of $CoCp_2$ is via the lower carbon ring, instead of through direct Co-Cr hybridization. This is different from most cases discussed in the literature for metallic films or adatoms [29].

B. Magnetic anisotropy

MAEs are important parameters for the SMMs, especially for their quantized spin excitations. In general, the MAE results from both the spin-orbit coupling (SOC, which gives the magnetocrystalline anisotropy) and magnetostatic dipole interaction (shape anisotropy). Through the total energy approach as $\mathrm{MAE} = E_x^{\mathrm{SOC}} - E_z^{\mathrm{SOC}}$, we obtained very small magnetocrystalline anisotropy for the clean AFM Cr(001) surface (−0.01 meV/Cr). The perturbative torque method [30,31] also gave the same result, as the SOC of Cr is much smaller than the crystal field. Considering that the shape anisotropy always gives a negative contribution to MAE for magnetic films, we may conclude that the easy axis of Cr atoms lies in the surface plane. For the free and the propped $CoCp_2$, the torque

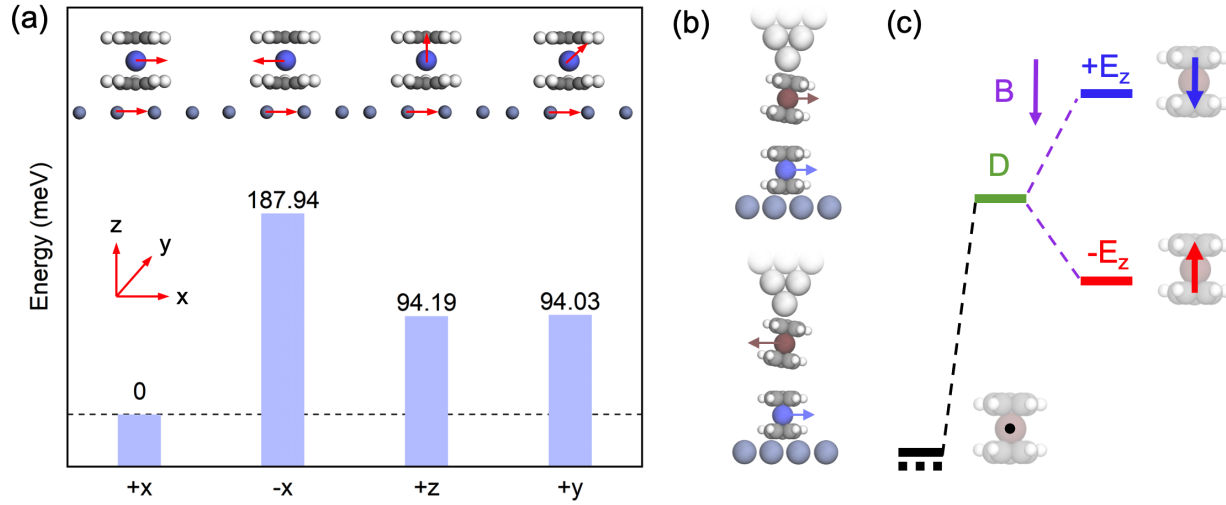

FIG. 3. (a) The energies of four noncollinear magnetic configurations shown in the inset. Red arrows denote directions of magnetic moments. The energy of the FM ground state has been subtracted for all configurations. (b) Schematic diagrams of two $NiCp_2$-tip/$CoCp_2$-surf systems. (c) Energy-level diagram of $NiCp_2$-tip ($S = 1$), showing single spin flip and Zeeman splitting. Solid and dashed black lines represent energy levels of two cases in (b). B, D and E_z are external magnetic field, MAE of $NiCp_2$-tip, and Zeeman energy, respectively. The black dot, red and blue arrows represent the spin state of $m_s = 0,\ +1,\ -1$, respectively.

method gives MAE of 0.60 and −0.22 meV, respectively. This indicates that the magnetic easy axis switches from along the molecular axis (z) to an in-plane (x) due to the interaction with the Cr(001) substrate. In order to explore the reasons, we follow the second perturbation approach [32]. The MAE can be expressed as

$$\mathrm{MAE} = \Delta E^{\uparrow\uparrow} + \Delta E^{\downarrow\downarrow} + \Delta E^{\uparrow\downarrow/\downarrow\uparrow}, \tag{1}$$

with

$$\begin{aligned}
\Delta E^{\uparrow\uparrow} &= \xi^2 \sum_{o^\uparrow, u^\uparrow} \frac{|\langle o^\uparrow|L_z|u^\uparrow\rangle|^2 - |\langle o^\uparrow|L_x|u^\uparrow\rangle|^2}{\varepsilon_u^\uparrow - \varepsilon_o^\uparrow} \\
\Delta E^{\downarrow\downarrow} &= \xi^2 \sum_{o^\downarrow, u^\downarrow} \frac{|\langle o^\downarrow|L_z|u^\downarrow\rangle|^2 - |\langle o^\downarrow|L_x|u^\downarrow\rangle|^2}{\varepsilon_u^\downarrow - \varepsilon_o^\downarrow} \\
\Delta E^{\uparrow\downarrow} &= \xi^2 \sum_{o^\uparrow, u^\downarrow} \frac{|\langle o^\uparrow|L_x|u^\downarrow\rangle|^2 - |\langle o^\uparrow|L_z|u^\downarrow\rangle|^2}{\varepsilon_u^\downarrow - \varepsilon_o^\uparrow}.
\end{aligned} \tag{2}$$

Here, ξ is the strength of SOC, arrows indicate spins, $\varepsilon_o^\uparrow$ and $\varepsilon_u^\uparrow$ are the energy levels of the occupied state and unoccupied state with spin up (or spin down for $\downarrow$), respectively. As shown in Fig. 2(d), states near the Fermi level are dominated by the $d_{xz/yz}$ orbitals in the majority spin channel for free $CoCp_2$. They give a positive contribution to MAE via the matrix element of L_z ($\langle xz|L_z|yz\rangle = 1$) through $\Delta E^{\uparrow\uparrow}$, resulting in a perpendicular anisotropy. When $CoCp_2$ is placed on the Cr surface, negative contributions develop from $\Delta E^{\uparrow\downarrow}$ due to the SOC interactions between the occupied majority spin and unoccupied minority spin $d_{xz/yz}$ states. The enhanced magnetic moment and in-plane anisotropy show that $CoCp_2$ on the Cr surface behaves somewhat like a free $NiCp_2$ with $S = 1$.

Furthermore, as $CoCp_2$ is approximately an S = 1 system on Cr(001), it hence can be described by a model Hamiltonian:

$$H_s = E_{ex}(\vec{S}\cdot\vec{S}_{\mathrm{Cr}}) - D\left(S_z^2\right) + E\left(S_x^2 - S_y^2\right) + H_{\mathrm{other}}, \tag{3}$$

where E_{ex} and $\vec{S}$ are the exchange energy and molecule spin, respectively. D and E are the two single-molecule magnetic anisotropy energies of $CoCp_2$. DFT calculations with SOC show that the exchange energy is about −94 meV, and D and E are −0.19 and −0.03 meV, respectively (see comparisons in Table S2) [19]. These parameters give the best fit to total energies of four magnetic configurations as seen in the inset of Fig 3(a). It is clear that the direction of magnetization of $CoCp_2$ is essentially pinned along the positive x axis, parallel to the magnetic moments of the topmost Cr atoms. Showing as a strong exchange bias effect, it costs about 188 meV for the spin of the $CoCp_2$ molecule to flip to the opposite direction. The energy costs for the spin to rotate to the z- or y axis are also high, about 94 meV. Even though the surface magnetization of Cr(001) might be somewhat overestimated by DFT calculations [33], we perceive that the exchange bias effect here is robust as the exchange energy between $CoCp_2$ and Cr(001) is very large.

Obviously, the large exchange bias effect with an exchange energy of −94 meV much surpasses the magnetic anisotropy energy of $CoCp_2$/Cr(001). The typical degeneracy between Kramers pairs is destroyed and the molecule spin is forced to be parallel to that of the substrate below the Néel temperature of Cr. This feature makes $CoCp_2$/Cr(001) suitable for magnetic molecule probe as it defines a stable direction of magnetization like coated tip but with a much weaker stray field and higher spatial resolution. We perceive that it is extremely useful for probing the single-molecule quantum spin states as one may mount the target molecule on the STM tip. Figure 3(b) shows this design with a $NiCp_2$ on tip (which is a $S = 1$ system with $D = 3.4$ meV [15]), probed by the

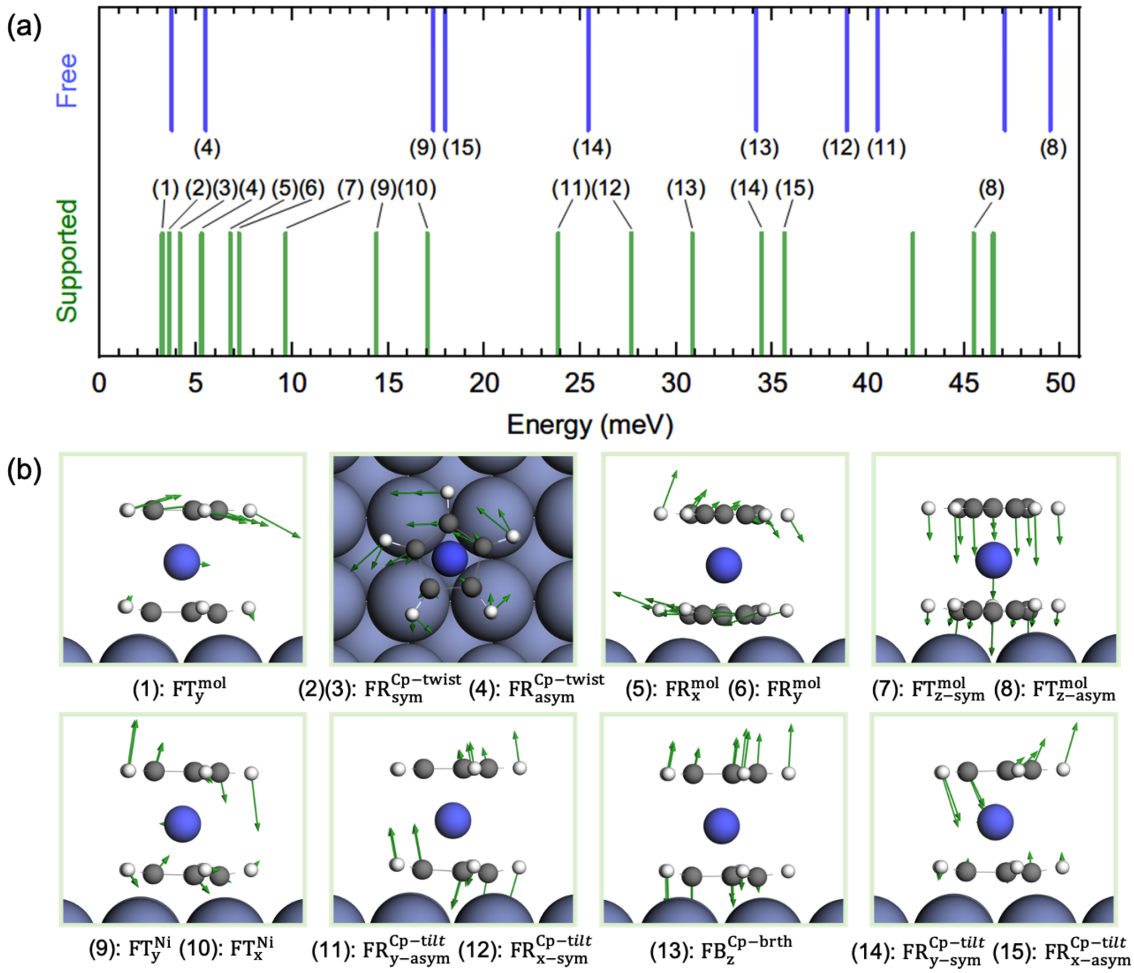

FIG. 4. The calculated vibration energies and corresponding modes below 50 meV. (a) Blue and green lines represent free and supported $CoCp_2$, respectively. For the free molecule, the similar modes are also marked with numbers. (b) (1)–(15) Vibration modes of the supported $CoCp_2$ molecule. Green arrows show the directions and amplitudes of atomic displacements.

$CoCp_2$-surf system. As the energy cost of flipping the spin of $CoCp_2$ is very high, the quantum spin spectrum of the target molecule can be obtained from Eq. (3) and is extremely simple, as depicted in Fig. 3(c). Interestingly, we may have two different $S_z = 0$ states, due to the exchange coupling between the two molecules. Since the spin direction of $CoCp_2$/Cr(001) is fixed, the tunneling current is expected to noticeably vary as the spin of $NiCp_2$ (or other target molecules) flips between different states. The STM and IETS features may hence provide more information such as lifetime or spin orientation of quantum spin states.

Note that the quantum spin Hamiltonian of free $CoCp_2$ or other $S = 1/2$ systems cannot have the MAE terms as in Eq. (3). Nevertheless, the interplay between spin-orbit coupling and local crystal field may still lead to sizable energy differences as spin aligns along different spatial axes. The common terms "up" and "down" for spin directions have no direct correspondence with real-space directions unless an external magnetic field or MAE is provided. Only with a positive MAE (e.g., 0.60 meV for free $CoCp_2$), the spin-up and -down states correspond to the $+z$ and $-z$ directions. The impossibility of having MAE in the $S = 1/2$ quantum Hamiltonian may somewhat prevent correct description for the coupling between $S = 1/2$ molecules and others if their MAEs are opposite in sign.

C. Vibrational spectrum of $CoCp_2$

As the vibration modes of $CoCp_2$ may still be excited in the tunneling process and contribute to the inelastic electron tunneling spectroscopy, we calculated the vibrational spectrum of free and supported $CoCp_2$ molecule with the finite difference approach. The energies of vibration modes for isolated and supported $CoCp_2$ below 50 meV are given in Fig. 4(a). Quantitatively, our vibration energies for the free $CoCp_2$ molecule agree well with results of previous theoretical calculations [34] as shown in Table S3 [19]. For the simplicity of comparing between the free and supported $CoCp_2$ molecule, we fixed all Cr atoms in our calculations for results in Fig. 4(a). We also calculated vibration modes with all the topmost Cr free to move. While many new modes appear in the energy range of 13 to 30 meV because of motions of Cr atoms, the vibration energies of $CoCp_2$ are not much affected according to the projected phonon density of states in Fig. S3 [19]. Obviously, the supported molecule has more vibrational modes in the low-energy region than the isolated case (see more

complete vibration energies in Table S4) [19]. The lowest vibration excitation energy of $CoCp_2$/Cr(001) is 3.23 meV. From the animations of several modes in Fig. 4(b), we may see that these modes such as FT_y^{mol}, $FR_{\mathrm{sym}}^{\mathrm{Cp-twist}}$, $FR_{x/y}^{\mathrm{mol}}$, and $FT_{z-\mathrm{sym}}^{\mathrm{mol}}$ are mainly associated with translation and rotation of the $CoCp_2$ molecule against the substrate. These vibrational modes are similar to previous theoretical results of $CoCp_2$/Cu [35] and $NiCp_2$/Ag [17]. With these energies, one may filter out the vibrational contributions of $CoCp_2$ from IETS for studies of other magnetic entities, e.g., the quantum spin states of single magnetic molecule or atom aforementioned.

IV. CONCLUSIONS

In summary, the structural, electronic, magnetic, and vibrational properties of $CoCp_2$ on the Cr(001) surface have been systematically studied using the first-principles calculations. The $CoCp_2$ molecule may remain stable on a Cr(001) surface and its magnetic moment and magnetic anisotropy energies are significantly affected because of the strong interaction with the substrate. Due to the exchange bias effect, the spin of $CoCp_2$ molecule is essentially pinned by Cr below the Néel temperature of Cr and a spin flip in $CoCp_2$ must overcome an energy barrier of ∼94 meV and an energy cost of ∼188 meV. This makes $CoCp_2$/Cr(001) suitable for probing quantum state of magnetic atoms or molecules in STM junctions. The involvement of low-energy vibration modes can be excluded with theoretical energies in hand, or via experiments without the target molecule on tip. This study provides guidelines to the design of functional tips or molecule sensors for studies of quantum spin states of small entities. Obviously, the same concept is applicable if one wants to use other metallocenes instead of $CoCp_2$. The only concern is the molecular structural instability as shown for $NiCp_2$ on Cr(001) because the metallic surface strongly hybridize with the low Cp ring. Furthermore, other AFM substrates such as thin magnetic oxide layers can also be used for the realization of the exchange bias effect. Nevertheless, FM substrates are not suitable as they may switch their magnetization in a strong magnetic field, which is needed for studies of quantum spin states of magnetic molecules.

ACKNOWLEDGMENTS

We thank Professor W. Ho at University of California, Irvine for insightful discussions. The work was supported by the National Science Foundation under Grant No. DMR-1809127 and by National Energy Research Scientific Computing Center.

[1] J. R. Friedman, M. Sarachik, J. Tejada, and R. Ziolo, Phys. Rev. Lett. **76**, 3830 (1996).
[2] S. J. Bartolome, F. Luis, and J. F. Fernández, *Molecular Magnets* (Springer, Heidelberg, 2014).
[3] W. Wernsdorfer and R. Sessoli, Science **284**, 133 (1999).
[4] M. Mannini *et al.*, Nature (London) **468**, 417 (2010).
[5] L. Bogani and W. Wernsdorfer, Nat. Mater. **7**, 179 (2008).
[6] Y. S. Ding, Y. F. Deng, and Y. Z. Zheng, Magnetochemistry **2**, 19, Unsp 40 (2016).
[7] E. Moreno-Pineda, C. Godfrin, F. Balestro, W. Wernsdorfer, and M. Ruben, Chem. Soc. Rev. **47**, 501 (2018).
[8] D. Shao and X.-Y. Wang, Chin. J. Chem. **38**, 1005 (2020).
[9] C. A. P. Goodwin, F. Ortu, D. Reta, N. F. Chilton, and D. P. Mills, Nature (London) **548**, 439 (2017).
[10] F. S. Guo, B. M. Day, Y. C. Chen, M. L. Tong, A. Mansikkamaki, and R. A. Layfield, Science **362**, 1400 (2018).
[11] M. Atzori, E. Morra, L. Tesi, A. Albino, M. Chiesa, L. Sorace, and R. Sessoli, J. Am. Chem. Soc. **138**, 11234 (2016).
[12] K. S. Pedersen, A. M. Ariciu, S. McAdams, H. Weihe, J. Bendix, F. Tuna, and S. Piligkos, J. Am. Chem. Soc. **138**, 5801 (2016).
[13] P. Wang, C.-Y. Luan, M. Qiao, M. Um, J. Zhang, Y. Wang, X. Yuan, M. Gu, J. Zhang, and K. Kim, Nat. Commun. **12**, 233 (2021).
[14] M. Ormaza *et al.*, Nano Lett. **17**, 1877 (2017).
[15] G. Czap, P. J. Wagner, F. Xue, L. Gu, J. Li, J. Yao, R. Q. Wu, and W. Ho, Science **364**, 670 (2019).
[16] B. Verlhac, N. Bachellier, L. Garnier, M. Ormaza, P. Abufager, R. Robles, M. L. Bocquet, M. Ternes, N. Lorente, and L. Limot, Science **366**, 623 (2019).
[17] G. Czap, P. J. Wagner, J. Li, F. Xue, J. Yao, R. Wu, and W. Ho, Phys. Rev. Lett. **123**, 106803 (2019).
[18] R. L. Stamps, J. Phys. D: Appl. Phys. **33**, R247 (2000).
[19] See Supplemental Material at http://link.aps.org/supplemental/10.1103/PhysRevB.105.064415 for details on properties of $NiCp_2$/Cr(001), results of $CoCp_2$/Cr(001) with seven Cr layers, effect of Hubbard U on magnetic states, more complete vibration energies, and phonon density of states.
[20] P. Habibi, C. Barreteau, and A. Smogunov, J. Phys.: Condens. Matter **25**, 146002 (2013).
[21] P. E. Blöchl, Phys. Rev. B **50**, 17953 (1994).
[22] G. Kresse and D. Joubert, Phys. Rev. B **59**, 1758 (1999).
[23] G. Kresse and J. Furthmüller, Phys. Rev. B **54**, 11169 (1996).
[24] G. Kresse and J. Furthmüller, Comput. Mater. Sci. **6**, 15 (1996).
[25] J. P. Perdew, K. Burke, and M. Ernzerhof, Phys. Rev. Lett. **77**, 3865 (1996).
[26] S. Grimme, J. Antony, S. Ehrlich, and H. Krieg, J. Chem. Phys. **132**, 154104 (2010).
[27] W. Tang, E. Sanville, and G. Henkelman, J. Phys.: Condens. Matter **21**, 084204 (2009).
[28] D. Khomskii, *Transition Metal Compounds* (Cambridge University Press, Cambridge, 2014) .
[29] A. J. Freeman and R.-q. Wu, J. Magn. Magn. Mater. **100**, 497 (1991).
[30] X. Wang, R. Wu, D.-s. Wang, and A. J. Freeman, Phys. Rev. B **54**, 61 (1996).
[31] R. Wu and A. J. Freeman, J. Magn. Magn. Mater. **200**, 498 (1999).

[32] D.-s. Wang, R. Wu, and A. J. Freeman, Phys. Rev. B **47**, 14932 (1993).

[33] J. A. Stroscio, D. T. Pierce, A. Davies, R. J. Celotta, and M. Weinert, Phys. Rev. Lett. **75**, 2960 (1995).

[34] Z. F. Xu, Y. M. Xie, W. L. Feng, and H. F. Schaefer, J. Phys. Chem. A **107**, 2716 (2003).

[35] L. Garnier, B. Verlhac, P. Abufager, N. Lorente, M. Ormaza, and L. Limot, Nano Lett. **20**, 8193 (2020).